Intricate Reaction Pathways on CH3NH3PbI3 Photocatalysts in Aqueous Solution Unraveled by Single-Particle Spectroscopy

Takeuchi, Aito
Kumabe, Yoshitaka
Tachikawa, Takashi

(Citation)
The Journal of Physical Chemistry Letters,14(10):2565-2572

(Issue Date)
2023-03-16

(Resource Type)
journal article

(Version)
Accepted Manuscript

(URL)
https://hdl.handle.net/20.500.14094/0100480921

Intricate Reaction Pathways on $CH_3NH_3PbI_3$ Photocatalysts in Aqueous Solution Unraveled by Single-Particle Spectroscopy

Aito Takeuchi,[†] Yoshitaka Kumabe,[‡] and Takashi Tachikawa[*†,‡]*

[†] Department of Chemistry, Graduate School of Science, Kobe University, 1-1 Rokkodai-cho, Nada-ku, Kobe 657-8501, Japan.

[‡] Molecular Photoscience Research Center, Kobe University, 1-1 Rokkodai-cho, Nada-ku, Kobe 657-8501, Japan.

AUTHOR INFORMATION

Corresponding Author

* tachikawa@port.kobe-u.ac.jp

ABSTRACT. Organic–inorganic hybrid perovskites such as $MAPbI_3$ ($MA^+ = CH_3NH_3^+$) have emerged as promising materials for solar cells and light-emitting devices. Despite their poor stability against moisture, perovskites work as hydrogen-producing photocatalysts or photosensitizers in perovskite-saturated aqueous solutions. However, the fundamental understanding of how chemical species or support materials in the solution affect the dynamics of the photogenerated charges in perovskites is still insufficient. In this study, we investigated the photoluminescence (PL) properties of $MAPbI_3$ nanoparticles in aqueous media at the single-particle level. A remarkable PL blinking phenomenon, along with significant decreases in the PL intensity and lifetime compared to those in ambient air, suggested temporal fluctuations in the trapping rates of photogenerated holes by chemical species (I^- and H_3PO_2) in the solution. Moreover, electron transfer from the excited $MAPbI_3$ to Pt-modified TiO_2 proceeds in a concerted fashion for photocatalytic hydrogen evolution under the dynamic solid–solution equilibrium condition.

TOC GRAPHICS

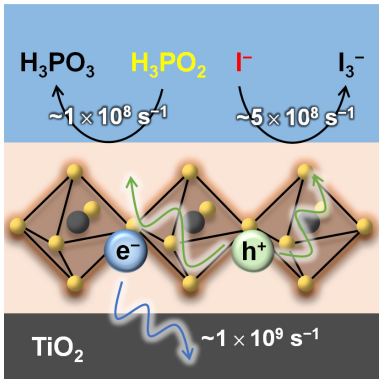

Metal halide perovskites such as $MAPbX_3$ ($MA^+ = CH_3NH_3^+$, $X^- = Cl^-$, Br^-, or I^-) and $CsPbX_3$ are expected to be utilized in photovoltaic and optoelectronic devices owing to their favorable properties, which include a strong absorption of visible light, long-length carrier diffusion, and a high photoluminescence (PL) quantum yield (QY).[1–5] Recently, these perovskites have been applied to various photochemical reactions.[6] For instance, Xu et al. reported that $CsPbBr_3$/graphene oxide (GO) acted as a photocatalyst for CO_2 reduction in ethyl acetate.[7] Yuan et al. found that ligand-capped $CsPbBr_3$ photocatalyzed stereoselective C–C bond formation under visible light irradiation.[8] Huang et al. reported, for the first time, the oxidation of alcohols to aldehydes using $FAPbBr_3$ ($FA^+ = CH(NH_2)^+$).[9]

In general, most perovskites decompose easily when in contact with H_2O or polar solvents.[10,11] However, Park et al. showed that $MAPbI_3$ is stable in aqueous solution by achieving a dynamic equilibrium between perovskite precipitates and a saturated solution containing their precursors.[12] Under this condition, the perovskites work as hydrogen (H_2)-producing photocatalysts by themselves (with Pt modification) or as photosensitizers when combined with Pt-modified TiO_2 (Pt/TiO_2) for H_2 evolution via HX splitting.[13] In addition, reduced GO, TiO_2, nickel carbide (Ni_3C), and black phosphorus have been employed as electron transport supports or co-catalysts to improve the photocatalytic activities.[14–16]

In aqueous solution systems, the electrons (e^-) and holes (h^+) generated in $MAPbI_3$ upon photoexcitation reduce protons (on materials such as Pt/TiO_2, where the deposited Pt nanoparticles act as H_2-producing co-catalysts) to produce H_2 and oxidize iodide ions (I^-) to eventually produce triiodide ions (I_3^-), as described by eqs 1–4.

$$MAPbI_3 + h\nu \rightarrow MAPbI_3(h^+) + MAPbI_3(e^-) \quad (1)$$

$$MAPbI_3(2h^+) + 3I^- \rightarrow MAPbI_3 + I_3^- \quad (2)$$

$$MAPbI_3(e^-) + Pt/TiO_2 \rightarrow MAPbI_3 + Pt/TiO_2(e^-) \quad (3)$$

$$Pt/TiO_2(2e^-) + 2H^+ \rightarrow Pt/TiO_2 + H_2 \quad (4)$$

I_3^- strongly absorbs visible light, which inhibits the light absorption by $MAPbI_3$. To achieve stable H_2 production, phosphinic acid (H_3PO_2) was added to the solution to reduce I_3^- to I^- (eq 5).[12]

$$I_3^- + H_3PO_2 + H_2O \rightarrow 3I^- + H_3PO_3 + 2H^+ \quad (5)$$

The time scale of interfacial charge transfer and lifetime of photogenerated charge carriers are significantly influenced by the structural properties (size, shape, degree of crystallinity, point defects, impurities, etc.) of semiconductor materials and determine their photocatalytic performance.[17] However, quantitative information related to the structural stability and charge carrier dynamics of perovskites in aqueous media is not yet available. A proper understanding of these fundamental principles could lead to their high and stable photocatalytic activities.

In this study, we elucidated the structural and charge carrier dynamics of $MAPbI_3$ nanoparticles in aqueous solution systems by analyzing their PL properties at the single-particle level. Single-molecule (single-particle) fluorescence spectroscopy allowed us to detect the emissions from a very few samples, ultimately individual molecules or particles, under a fluorescence microscope. It has been employed to solve the dynamic structural and chemical conversions over organo-lead halide perovskites, which are usually hidden in ensemble- and time-averaging bulk experiments.[18,19]

For single-particle observations, cuboid-shaped $MAPbI_3$ nanoparticles were synthesized by adding a poor solvent (dichloromethane) to a solution of precursors (MAI and PbI_2) in a good solvent (γ-butyrolactone) at room temperature, followed by mixing with a solution of capping ligands (*n*-octylamine, OA) (Figure 1a).[20] The steady-state diffuse reflectance spectrum of the nanoparticles in toluene shows a continuous absorption band due to interband transition with an edge at ~765 nm (Figure 1b). The maximum PL emission appeared at ~765 nm, indicating that the observed PL originates from the radiative recombination of photogenerated electrons and holes in the $MAPbI_3$ (Figure 1b).[21,22] The powder X-ray diffraction (XRD) pattern indicates that the OA-capped $MAPbI_3$ nanoparticles possess a tetragonal structure (Figures 1c and S1).[23] From the Scherrer equation,[24] the crystallite size for the (220) plane was calculated to be ~31 nm. This value is reasonable compared with the statistical data of short-axis lengths (~53 nm) obtained from field emission scanning electron microscopy (FE-SEM) images (Figure 1a). The results of further structural and elemental analyses were reported in our previous paper.[20]

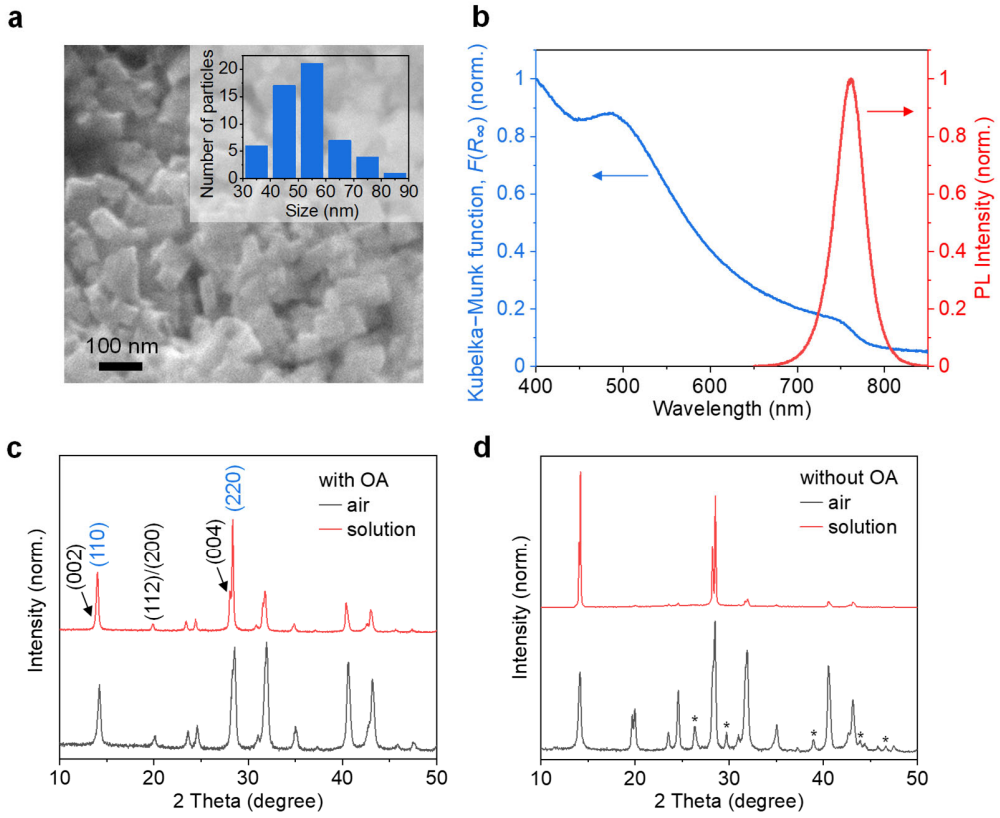

Figure 1. (a) FE-SEM image of OA-capped $MAPbI_3$ nanoparticles and (inset) particle size distribution. (b) Steady-state diffuse reflectance and PL spectra of OA-capped $MAPbI_3$ nanoparticles dispersed in toluene. (c,d) XRD patterns of $MAPbI_3$ nanoparticles synthesized with (c) and without (d) OA. The particles were dried in ambient air (lower) or immersed in $MAPbI_3$-saturated HI-H_3PO_2 solution (upper). Asterisks indicate characteristic peaks of hydrated species.

To examine the stability of the perovskite structure in aqueous solution, we exposed $MAPbI_3$ nanoparticles to $MAPbI_3$-saturated HI solutions with and without H_3PO_2 and then measured the XRD patterns. As shown in Figures 1c and S2, only the diffraction peaks indexed to the (110) and (220) planes were significantly enhanced after treatment. The crystallite size parallel to the (220) plane increased to ~66 nm on average, suggesting that the $MAPbI_3$ crystals tend to grow selectively along the [002] direction in the solution (Figure S1). This anisotropic growth may have been due to the adsorption of OA and/or excess MA^+ in solution on the (110) facets, leading to a reduction

in their surface energy.[25–27] On the other hand, after being exposed to ambient air for a while, the $MAPbI_3$ nanoparticles synthesized without OA exhibited several additional diffraction peaks, including those at ~26.3°, ~29.7°, and ~39.0°, which could be assigned to $MAPbI_3$ hydrates (Figure 1d).[28,29] Interestingly, only the peaks of pure $MAPbI_3$ were observed after exposing the $MAPbI_3$ hydrates to the $MAPbI_3$-saturated HI solution. This result demonstrates that the $MAPbI_3$ structure did not decompose in the aqueous solution, but rather improved the crystallinity as a result of the dynamic equilibrium. The capping ligands work not only in obtaining homogeneous nanoparticles with a controlled size and shape, as is evident from FE-SEM image of $MAPbI_3$ nanoparticles synthesized without OA (Figure S3), but also in suppressing the hydration of $MAPbI_3$, presumably through a hydrogen bonding interaction with surface iodide atoms.[30] Fourier transform infrared (FTIR) spectra confirmed the presence of the OA molecules on the surface of $MAPbI_3$ nanoparticles even after immersing in $MAPbI_3$-saturated HI-H_3PO_2 solution (Figure S4).

The PL properties of the OA-capped $MAPbI_3$ nanoparticles were first investigated using a wide-field and confocal microscope system after depositing the particles on a quartz cover glass and immersing them in $MAPbI_3$-saturated HI-H_3PO_2 solution (Figure 2a). Figure 2b shows the typical PL spectra of single OA-capped $MAPbI_3$ nanoparticles (or few-particle aggregates) exposed to ambient air and the aqueous solution under 405 nm excitation. The peak wavelengths (760 ± 5 nm) observed under the two conditions were almost the same, suggesting that no significant structural changes such as hydration or particle size decrease[31] occurred during the observation period. Notably, approximately half the bare $MAPbI_3$ nanoparticles in ambient air exhibited the PL peak wavelengths same as those (760 ± 5 nm) of OA-capped ones, while the others possess the peaks blue-shifted by approximately 10–20 nm (0.02–0.04 eV), possibly due to hydration (Figure S5).[32,33] After immersion in the solution, however, no such blue shift was observed. These results

imply the dissolution and recrystallization of hydrated $MAPbI_3$ nanoparticles, leading to the formation of $MAPbI_3$ with a pristine crystal structure under dynamic equilibrium, in accordance with the XRD results (Figure 1d). Another possible explanation is that blue-shifted PL was almost completely quenched due to further hydration or decomposition. Thus, OA-capped $MAPbI_3$ nanoparticles were employed herein for the long-term PL observation of single particles.

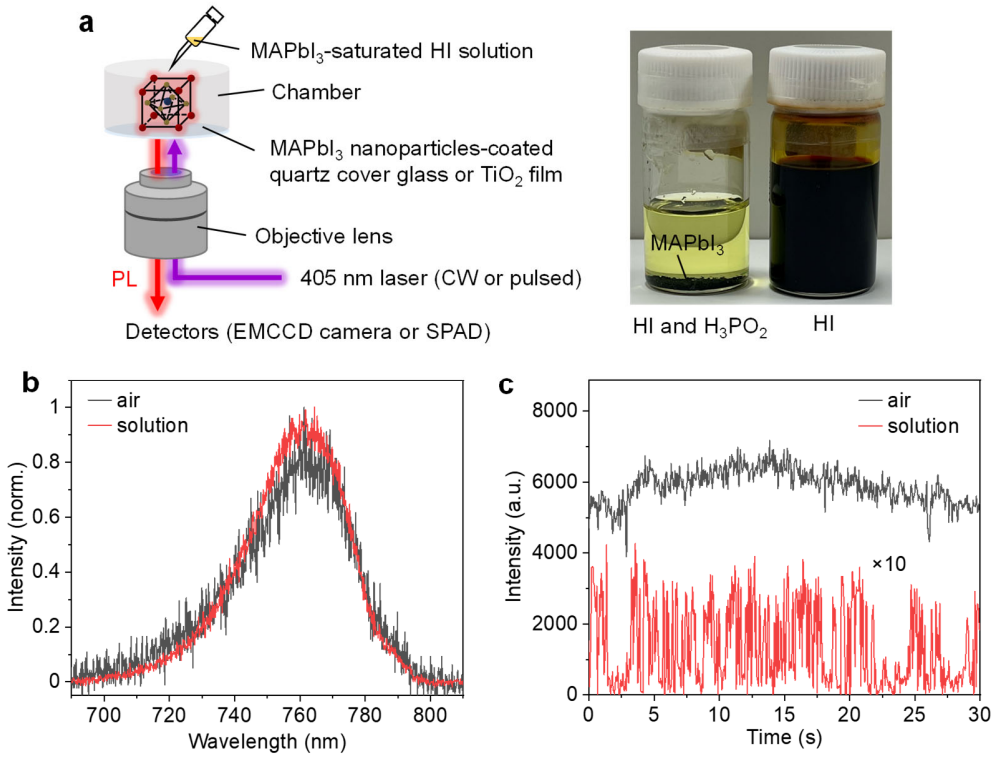

Figure 2. (a) Schematic of the PL microscopy measurement system. Photograph shows the $MAPbI_3$-saturated HI aqueous solutions with (left) and without (right) H_3PO_2 that reduces I_3^- to I^-. (b,c) Typical PL spectra (b) and intensity trajectories (c) of single OA-capped $MAPbI_3$ nanoparticles dispersed on quartz cover glasses. The samples were exposed to ambient air (black) or to $MAPbI_3$-saturated HI-H_3PO_2 solution (red).

After being exposed to the $MAPbI_3$-saturated HI-H_3PO_2 solution, most of the particles exhibited the so-called PL blinking, where the particle emitted in an intermittent on-and-off fashion (Figures 2c, S6, and Supporting Movies S1 and S2).[34] This blinking phenomenon is commonly observed

for single semiconductor nanostructures including metal halide perovskites[18,35–38] and mostly originates from the suppression of radiative recombination due to the stochastic trapping of charge carriers by surface defects or the Auger recombination, which quenches the emission via the transfer of exciton energy to the third carrier in the particle.[39,40] The intriguing blinking features of the $MAPbI_3$ nanoparticles will be discussed later.

To investigate the charge carrier dynamics of $MAPbI_3$ nanoparticles, time-resolved PL measurements were carried out on individual particles. The PL decay profiles were fitted by a single or double exponential decay function to determine the PL lifetimes and their contributions (Figure 3a). Under the air condition, the faster component (τ_1) (~33 ns) is assigned to the trapping of charge carriers by surface defects, and the slower component (τ_2) (~139 ns) is assigned to the radiative recombination of charge carriers through intraparticle diffusion (Figures 3b and S7, and Table 1).[2,41] The wide distributions of τ values would be mainly attributed to the variation in the particle size because a linear relationship between τ_1 and τ_2 obtained for the same particle in air (Figure S8) implied that both processes had a size-dependent characteristic.[20] After being exposed to the $MAPbI_3$-saturated HI-H_3PO_2 solution, the PL lifetimes decreased by one order of magnitude or more (τ_1 of ~2.1 ns and τ_2 of ~8.6 ns) (Figure 3c). This result is consistent with the weakened PL and implies that there were additional nonradiative pathways caused by the chemical species in the aqueous solution. For the bare nanoparticles in ambient air, τ_1 was shortened to ~4.2 ns (Figure S9), possibly as a result of partial hydration, while τ_2 (~32 ns) was very close to the τ_1 value (~33 ns) of the OA-capped sample, which was attributed to defect-mediated recombination, as mentioned above. In $MAPbI_3$-saturated HI-H_3PO_2 solution, much shorter components (~0.4 ns) appeared for the bare nanoparticles, suggesting that the hole transfer was accelerated through direct interactions with I^- and H_3PO_2.

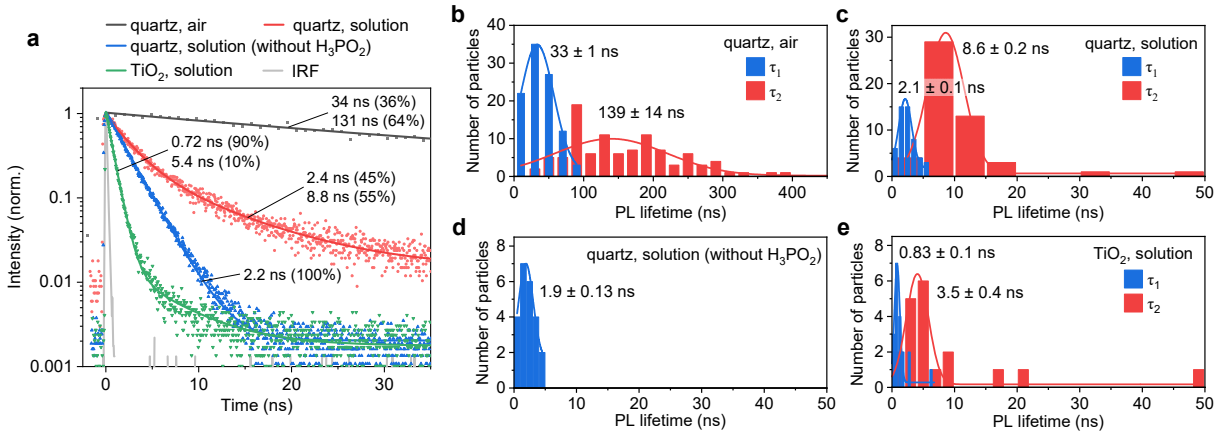

Figure 3. (a) PL decay profiles (dots) observed for typical single $MAPbI_3$ nanoparticles during 405-nm pulsed laser irradiation. The solid lines show the nonlinear least-squares fittings to exponential functions. The whole profile obtained for the particle on quartz in air is given in Figure S7. (b–e) Histograms of lifetimes for individual nanoparticles dispersed on quartz cover glasses (b–d) and a TiO_2-coated quartz cover glass (e). The samples were exposed to ambient air (b) or to $MAPbI_3$-saturated HI solution with (c,e) or without (d) H_3PO_2. The solid lines show the nonlinear least-squares fittings to Gaussian functions.

Table 1. Average PL Lifetimes of OA-Capped $MAPbI_3$ Nanoparticles and Their Related Reaction Processes

conditions	$\langle\tau_1\rangle$ (reaction process)	$\langle\tau_2\rangle$ (reaction process)
quartz, air	33 ns (e^-/h^+ trapping by surface defects)	139 ns (radiative recombination)
quartz, solution	2.1 ns (h^+ transfer to I^-)	8.6 ns (h^+ transfer to H_3PO_2)
TiO_2, solution	0.83 ns (e^- transfer to TiO_2)	3.5 ns (h^+ transfer to I^-/H_3PO_2)

To identify the chemical species that induced nonradiative charge-transfer processes, we prepared a $MAPbI_3$-saturated HI solution without H_3PO_2 and carried out the same measurements. As demonstrated in Figure 3d, only one component (~1.9 ns) was observed, suggesting that the fast (~2.1 ns) and slow (~8.6 ns) components in the presence of H_3PO_2 are assignable to hole transfers to I^- and H_3PO_2, respectively. The observed overall rate is given as $k_{obs} = \langle n \rangle \times k'_{HT}$, where $\langle n \rangle$ is the average number of bound acceptors per particle, and k'_{HT} is the intrinsic hole transfer rate. The $\langle n \rangle$ value is basically dependent on the concentration and adsorption constant (i.e., the interaction between the $MAPbI_3$ and hole acceptors) of the hole acceptors in solution at low surface coverage values. The molar ratio of I^-:H_3PO_2 in the solution was 3.3:1.0. Considering the pK_a values of HI (−10) and H_3PO_2 (1.23)[42] and the pH of the solution (approx. −0.7), the H_3PO_2 was almost fully protonated. Therefore, I^- ions were preferentially adsorbed on the cationic sites on the surface of the $MAPbI_3$ because of electrostatic interactions, which effectively captured holes. A further discussion of k'_{HT} within the framework of the Marcus theory is provided in Supporting Note S1.

To gain further insight into the design of the photocatalytic H_2 production system, we examined the PL properties of OA-capped $MAPbI_3$ nanoparticles on the TiO_2 film formed on the quartz cover glass (Figure S10). Figure S11 shows the PL trajectories captured under the air and solution conditions. In air, the $MAPbI_3$ nanoparticles exhibited blinking, but were quickly photobleached. Because the conduction band (CB) of TiO_2 is more positive than that of $MAPbI_3$, photogenerated electrons in $MAPbI_3$ were quickly transferred to the TiO_2, which may result in the accumulation of excess holes that escaped the recombination processes, thus leading to the decomposition of the perovskite structure.[43,44] This result also indicates that holes in the valence band (VB) of $MAPbI_3$ are transferred to I^- or H_3PO_2, which plays a crucial role in maintaining the overall charge balance

in the perovskite to avoid undesired photodegradation and catalyze the HI splitting reaction for H_2 generation.[13]

Time-resolved measurements revealed that the PL lifetimes of the OA-capped $MAPbI_3$ nanoparticles on TiO_2 were much shorter than those on quartz when exposed to $MAPbI_3$-saturated HI-H_3PO_2 solutions (Figures 3a, c, and e). This is because electron transfer to the TiO_2 is the dominant competitive process. From these results, we can assign the faster component (<1 ns) to electron transfer to TiO_2 and the slower component (3.5 ns) to hole transfer to I^- and/or H_3PO_2 (Figure 3e). The electron/hole transfer rates can be calculated from $k_{ET/HT} = <\tau_{acceptor}>^{-1}$, where $<\tau_{acceptor}>$ is the specific lifetime component for the electron/hole transfer to the acceptors (Table 1). The hole transfer rate for I^- (4.8×10^8 s^{-1}) is approximately one-tenth of the hole transfer rate to the hole transport layers (Spiro-OMeTAD and PEDOT:PSS) of perovskite solar cells.[45,46] This is possibly because the charge transfer between a solid and solid interface is more efficient than that between liquid and solid interfaces owing to stronger electronic couplings with hole acceptors. Improving the hole transfer rate would be crucial to improve the stability of perovskites and thus enhance their photocatalytic activities.

The rate of electron transfer from OA-capped $MAPbI_3$ nanoparticles to TiO_2 ($<\tau_1>^{-1} = 1.2 \times 10^9$ s^{-1}) in $MAPbI_3$-saturated HI-H_3PO_2 solution is comparable to that reported for a $MAPbI_3/TiO_2$ film in air.[47] The capping ligands or stabilizing agents can greatly improve the durability and physicochemical properties of nanoparticles in solution but often limit the accessibility of substrates on the surface and hinder the direct charge transfer between the reactants and active sites.[48–50] This is as true for the present systems, according to the fact that the rate of electron transfer from bare $MAPbI_3$ nanoparticles to TiO_2 in the solution was determined to be 2.2×10^9

s^{-1} (Figure S12). To examine the relationship between interfacial charge transfer dynamics and photocatalytic performance, H_2 generation via visible-light-driven HI splitting was tested. As demonstrated in Figure 4a, $MAPbI_3$ nanoparticles both with and without OA showed stable H_2 production by mixing with Pt-modified TiO_2 nanoparticles (Pt/TiO_2) (Figure S13). Relative H_2 production efficiencies of bare and OA-capped samples follow the relative rates of electron transfer (i.e., $2.2 \times 10^9\ s^{-1}/1.2 \times 10^9\ s^{-1} = 1.8$), revealing the critical role of surface-capping ligands in determining the photochemical activity of the $MAPbI_3/TiO_2$ hybrid systems.

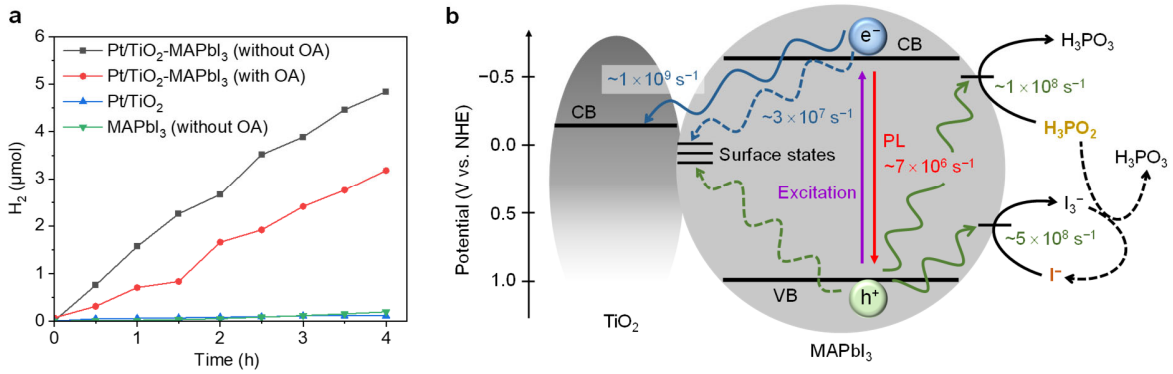

Figure 4. (a) Photocatalytic H_2 evolution from the samples in $MAPbI_3$-saturated HI-H_3PO_2 solutions under visible light irradiation (center wavelength = 565 nm; intensity = 50 mW cm^{-2}). 10-mg $MAPbI_3$ nanoparticles synthesized with (red) or without (black) OA were mixed with 5-mg Pt/TiO_2 in 5 mL Ar-saturated solution. Pt/TiO_2 (5 mg; blue) and bare $MAPbI_3$ nanoparticles (10 mg; green) were used for control experiments. (b) Energy diagram of charge transfer processes on the OA-capped $MAPbI_3/TiO_2$ system in aqueous solution.

Figure 4b illustrates the energy diagram and charge transfer processes of the $MAPbI_3/TiO_2$ system in aqueous solution with representative reaction rates. First, electrons and holes are generated in the CB and VB of $MAPbI_3$, respectively, upon excitation with photons with energies larger than the bandgap. The electrons are then transferred to the CB of TiO_2 located at −0.12 V vs. NHE[51] (~$10^9\ s^{-1}$), followed by hole transfer to I^- in aqueous solution (10^8–$10^9\ s^{-1}$). At the same

time, trap-mediated recombination, or hole transfer to H_3PO_2 occurs at a slower rate (~10^8 s^{-1}). Without TiO_2, the electrons in the $MAPbI_3$ would be transferred to molecular oxygen adsorbed on the surface.[43,52] The surviving electrons and holes recombine radiatively (~10^7 s^{-1}). Because these reaction rates temporally fluctuate, as suggested by the PL blinking, minor (slower) pathways are clearly recognized in single-particle experiments.

Finally, we discuss the origin of the PL blinking observed for the OA-capped $MAPbI_3$ nanoparticles in solution. There are two possibilities. The PL blinking might have been the result of stochastic charge trapping by surface defects and adsorbates or Auger recombination-assisted quenching. However, the contribution of Auger recombination was relatively small based on the fact that no remarkable blinking was observed when the excitation power was increased (Figure S14).[53] This conclusion is also supported by a statistical analysis of the blinking characteristics (see Supporting Note S2).

The OA-capped $MAPbI_3$ nanoparticles in air showed no or less blinking, while those in aqueous solution exhibited many blinking cycles with on and off times (τ_{on} and τ_{off}) on a time scale of milliseconds to seconds. These results suggest that the chemical species in the solution captured the charge carriers at a higher turnover rate. In addition, the nanoparticles in solution without H_3PO_2 did not show distinct blinking at a frame rate of 20 fps, implying that H_3PO_2 is essential for blinking on a time scale of tens of milliseconds to seconds (Figure 5a). The fluorescence lifetime-intensity distribution (FLID) map shows an almost linear relationship between them, indicating a temporal fluctuation of the hole transfer dynamics (Figure 5b).

Based on the results of the blinking analysis, we propose a possible blinking mechanism, as shown in Figure 5c. $MAPbI_3$ nanoparticles emit PL (the on-state) when H_3PO_2 molecules, which

are ineffective hole acceptors, temporarily occupy the adsorption sites on the $MAPbI_3$ surface. Meanwhile, the $MAPbI_3$ nanoparticles do not emit PL (the off-state) when I^- ions, which are effective hole acceptors, are predominantly adsorbed on the surface. Our interpretation fits well with the model that the opening and closing of nonradiative channels in luminescent quantum dots are the result of fluctuations in the adsorbate binding to the particle surface.[54] This dynamic fluctuation is vital not only for the PL blinking phenomenon but also for the single turnover of the catalyzed conversion of substrates on solid (photo)catalysts.[55,56] A more complete understanding of such substrate-induced fluctuation events will provide fundamental insights into (photo)catalytic behaviors in dynamic equilibrium systems, which are often inaccessible in ensemble-averaged measurements.

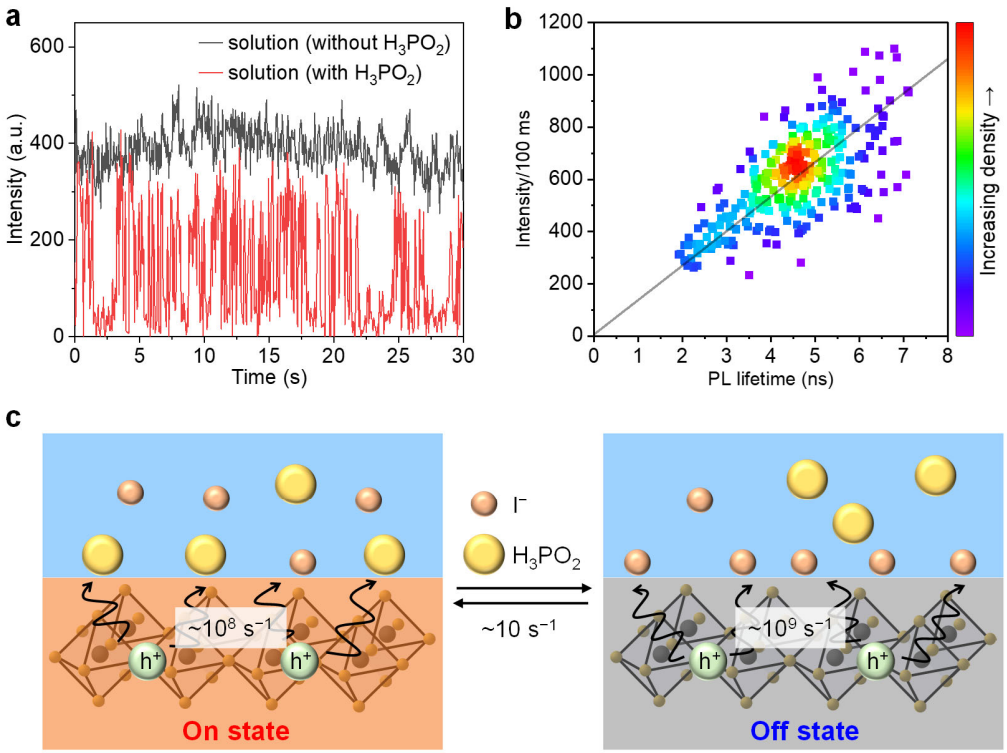

Figure 5. (a) PL intensity trajectories of single OA-capped $MAPbI_3$ nanoparticles in $MAPbI_3$-saturated HI solutions with (red) and without (black) H_3PO_2. (b) A typical FLID map obtained for

a single OA-capped $MAPbI_3$ nanoparticle in $MAPbI_3$-saturated HI-H_3PO_2 solution. The solid line indicates the fit of the linear relationship between them. (c) Mechanistic illustration of the blinking behavior under dynamic solid–solution equilibrium condition.

In conclusion, we successfully characterized the structural and PL properties of $MAPbI_3$ nanoparticles in aqueous solution. To the best of our knowledge, this is the first example of PL from metal halide perovskites in aqueous solutions. The perovskite structure is stable, especially with the aid of capping ligands, in the perovskite-saturated HI solution and recovered from decomposed ones, as revealed by the XRD data. Based on the remarkable PL blinking, as well as the decreased PL intensity and lifetimes for OA-capped $MAPbI_3$ nanoparticles in $MAPbI_3$-saturated HI-H_3PO_2 solution, we propose that the temporal fluctuation of the charge carrier trapping originates from the stochastic and competitive adsorption of hole acceptors, I^- and H_3PO_2, where the former is a more effective species under the present conditions. We further note that interfacial electron transfer from excited $MAPbI_3$ to the TiO_2 support competes with these hole transfer processes and eventually determines the efficiency of photocatalytic H_2 evolution. Our single-particle approach for investigating the intricate nature of photocatalysis in dynamic solid–solution equilibrium will provide a design principle for a new type of (photo)catalytic system apart from conventional homogeneous and heterogeneous systems.

ASSOCIATED CONTENT

Supporting Information. Experimental methods, additional results and discussion. This material is available free of charge via the Internet at http://pubs.acs.org.

AUTHOR INFORMATION

Corresponding Author

* Takashi Tachikawa: tachikawa@port.kobe-u.ac.jp.

Notes

The authors declare no competing financial interest.

ACKNOWLEDGMENT

This work was supported by JSPS KAKENHI (grant Nos. JP18H01944, JP20H04673, and JP21H02049).

REFERENCES

(1) Kojima, A.; Teshima, K.; Shirai, Y.; Miyasaka, T. Organometal Halide Perovskites as Visible-Light Sensitizers for Photovoltaic Cells. *J. Am. Chem. Soc.* **2009**, *131*, 6050–6051.

(2) Shi, D.; Adinolfi, V.; Comin, R.; Yuan, M.; Alarousu, E.; Buin, A.; Chen, Y.; Hoogland, S.; Rothenberger, A.; Katsiev, K.; Losovyj, Y.; Zhang, X.; Dowben, P. A.; Mohammed, O. F.; Sargent, E. H.; Bakr, O. M. Low Trap-State Density and Long Carrier Diffusion in Organolead Trihalide Perovskite Single Crystals. *Science* **2015**, *347*, 519–522.

(3) Stranks, S. D.; Eperon, G. E.; Grancini, G.; Menelaou, C.; Alcocer, M. J. P.; Leijtens, T.; Herz, L. M.; Petrozza, A.; Snaith, H. J. Electron-Hole Diffusion Lengths Exceeding 1 Micrometer in an Organometal Trihalide Perovskite Absorber. *Science* **2013**, *342*, 341–344.

(4) Lee, M. M.; Teuscher, J.; Miyasaka, T.; Murakami, T. N.; Snaith, H. J. Efficient Hybrid Solar Cells Based on Meso-Superstructured Organometal Halide Perovskites. *Science* **2012**, *338*, 643–647.

(5) Tan, Z.-K.; Moghaddam, R. S.; Lai, M. L.; Docampo, P.; Higler, R.; Deschler, F.; Price, M.; Sadhanala, A.; Pazos, L. M.; Credgington, D.; Hanusch, F.; Bein, T.; Snaith, H. J.; Friend, R. H. Bright Light-Emitting Diodes Based on Organometal Halide Perovskite. *Nat. Nanotechnol.* **2014**, *9*, 687–692.

(6) Huang, H.; Pradhan, B.; Hofkens, J.; Roeffaers, M. B. J.; Steele, J. A. Solar-Driven Metal Halide Perovskite Photocatalysis: Design, Stability, and Performance. *ACS Energy Lett.* **2020**, *5*, 1107–1123.

(7) Xu, Y.-F.; Yang, M.-Z.; Chen, B.-X.; Wang, X.-D.; Chen, H.-Y.; Kuang, D.-B.; Su, C.-Y. A $CsPbBr_3$ Perovskite Quantum Dot/Graphene Oxide Composite for Photocatalytic CO_2 Reduction. *J. Am. Chem. Soc.* **2017**, *139*, 5660–5663.

(8) Yuan, Y.; Zhu, H.; Hills-Kimball, K.; Cai, T.; Shi, W.; Wei, Z.; Yang, H.; Candler, Y.; Wang, P.; He, J.; Chen, O. Stereoselective C−C Oxidative Coupling Reactions Photocatalyzed by Zwitterionic Ligand Capped $CsPbBr_3$ Perovskite Quantum Dots. *Angew. Chem. Int. Ed.* **2020**, *59*, 22563–22569.

(9) Huang, H.; Yuan, H.; Janssen, K. P. F.; Solís-Fernández, G.; Wang, Y.; Tan, C. Y. X.; Jonckheere, D.; Debroye, E.; Long, J.; Hendrix, J.; Hofkens, J.; Steele, J. A.; Roeffaers, M. B. J. Efficient and Selective Photocatalytic Oxidation of Benzylic Alcohols with Hybrid Organic–Inorganic Perovskite Materials. *ACS Energy Lett.* **2018**, *3*, 755–759.

(10) De Wolf, S.; Holovsky, J.; Moon, S.-J.; Loper, P.; Niesen, B.; Ledinsky, M.; Haug, F.-J.; Yum, J.-H.; Ballif, C. Organometallic Halide Perovskites: Sharp Optical Absorption Edge and Its Relation to Photovoltaic Performance. *J. Phys. Chem. Lett.* **2014**, *5*, 1035–1039.

(11) Han, Y.; Meyer, S.; Dkhissi, Y.; Weber, K.; Pringle, J. M.; Bach, U.; Spiccia, L.; Cheng, Y.-B. Degradation Observations of Encapsulated Planar $CH_3NH_3PbI_3$ Perovskite Solar Cells at High Temperatures and Humidity. *J. Mater. Chem. A* **2015**, *3*, 8139–8147.

(12) Park, S.; Chang, W. J.; Lee, C. W.; Park, S.; Ahn, H.-Y.; Nam, K. T. Photocatalytic Hydrogen Generation from Hydriodic Acid Using Methylammonium Lead Iodide in Dynamic Equilibrium with Aqueous Solution. *Nat. Energy* **2017**, *2*, 16185.

(13) Wang, X.; Wang, H.; Zhang, H.; Yu, W.; Wang, X.; Zhao, Y.; Zong, X.; Li, C. Dynamic Interaction between Methylammonium Lead Iodide and TiO_2 Nanocrystals Leads to Enhanced Photocatalytic H_2 Evolution from HI Splitting. *ACS Energy Lett.* **2018**, *3*, 1159–1164.

(14) Wu, Y.; Wang, P.; Zhu, X.; Zhang, Q.; Wang, Z.; Liu, Y.; Zou, G.; Dai, Y.; Whangbo, M.-H.; Huang, B. Composite of $CH_3NH_3PbI_3$ with Reduced Graphene Oxide as a Highly Efficient and Stable Visible-Light Photocatalyst for Hydrogen Evolution in Aqueous HI Solution. *Adv. Mater.* **2018**, *30*, 1704342.

(15) Zhao, Z.; Wu, J.; Zheng, Y.-Z.; Li, N.; Li, X.; Tao, X. Ni_3C-Decorated $MAPbI_3$ as Visible-Light Photocatalyst for H_2 Evolution from HI Splitting. *ACS Catal.* **2019**, *9*, 8144–8152.

(16) Li, R.; Li, X.; Wu, J.; Lv, X.; Zheng, Y.-Z.; Zhao, Z.; Ding, X.; Tao, X.; Chen, J.-F. Few-Layer Black Phosphorus-on-$MAPbI_3$ for Superb Visible-Light Photocatalytic Hydrogen Evolution from HI Splitting. *Appl. Catal. B Environ.* **2019**, *259*, 118075.

(17) Tachikawa, T.; Fujitsuka, M.; Majima, T. Mechanistic Insight into the TiO_2 Photocatalytic Reactions: Design of New Photocatalysts. *J. Phys. Chem. C* **2007**, *111*, 5259–5275.

(18) Tachikawa, T.; Karimata, I.; Kobori, Y. Surface Charge Trapping in Organolead Halide Perovskites Explored by Single-Particle Photoluminescence Imaging. *J. Phys. Chem. Lett.* **2015**, *6*, 3195–3201.

(19) Park, Y.-S.; Guo, S.; Makarov, N. S.; Klimov, V. I. Room Temperature Single-Photon Emission from Individual Perovskite Quantum Dots. *ACS Nano* **2015**, *9*, 10386–10393.

(20) Karimata, I.; Tachikawa, T. In Situ Exploration of the Structural Transition during Morphology- and Efficiency-Conserving Halide Exchange on a Single Perovskite Nanocrystal. *Angew. Chem. Int. Ed.* **2021**, *60*, 2548–2553.

(21) D'Innocenzo, V.; Grancini, G.; Alcocer, M. J. P.; Kandada, A. R. S.; Stranks, S. D.; Lee, M. M.; Lanzani, G.; Snaith, H. J.; Petrozza, A. Excitons versus Free Charges in Organo-Lead Tri-Halide Perovskites. *Nat. Commun.* **2014**, *5*, 4586.

(22) Herz, L. M. How Lattice Dynamics Moderate the Electronic Properties of Metal-Halide Perovskites. *J. Phys. Chem. Lett.* **2018**, *9*, 6853–6863.

(23) Jang, D. M.; Park, K.; Kim, D. H.; Park, J.; Shojaei, F.; Kang, H. S.; Ahn, J. P.; Lee, J. W.; Song, J. K. Reversible Halide Exchange Reaction of Organometal Trihalide Perovskite Colloidal Nanocrystals for Full-Range Band Gap Tuning. *Nano Lett.* **2015**, *15*, 5191–5199.

(24) Patterson, A. L. The Scherrer Formula for X-Ray Particle Size Determination. *Phys. Rev.* **1939**, *56*, 978–982.

(25) Jao, M.-H.; Lu, C.-F.; Tai, P.-Y.; Su, W.-F. Precise Facet Engineering of Perovskite Single Crystals by Ligand-Mediated Strategy. *Cryst. Growth Des.* **2017**, *17*, 5945–5952.

(26) Zhang, J.; Wang, K.; Yao, Q.; Yuan, Y.; Ding, J.; Zhang, W.; Sun, H.; Shang, C.; Li, C.; Zhou, T.; Pang, S. Carrier Diffusion and Recombination Anisotropy in the $MAPbI_3$ Single Crystal. *ACS Appl. Mater. Interfaces* **2021**, *13*, 29827–29834.

(27) Yin, J.; Cortecchia, D.; Krishna, A.; Chen, S.; Mathews, N.; Grimsdale, A. C.; Soci, C. Interfacial Charge Transfer Anisotropy in Polycrystalline Lead Iodide Perovskite Films. *J. Phys. Chem. Lett.* **2015**, *6*, 1396–1402.

(28) Leguy, A. M. A.; Hu, Y.; Campoy-Quiles, M.; Alonso, M. I.; Weber, O. J.; Azarhoosh, P.; van Schilfgaarde, M.; Weller, M. T.; Bein, T.; Nelson, J.; Docampo, P.; Barnes, P. R. F. Reversible Hydration of $CH_3NH_3PbI_3$ in Films, Single Crystals, and Solar Cells. *Chem. Mater.* **2015**, *27*, 3397–3407.

(29) Askar, A. M.; Bernard, G. M.; Wiltshire, B.; Shankar, K.; Michaelis, V. K. Multinuclear Magnetic Resonance Tracking of Hydro, Thermal, and Hydrothermal Decomposition of $CH_3NH_3PbI_3$. *J. Phys. Chem. C* **2017**, *121*, 1013–1024.

(30) De Roo, J.; Ibáñez, M.; Geiregat, P.; Nedelcu, G.; Walravens, W.; Maes, J.; Martins, J. C.; Van Driessche, I.; Kovalenko, M. V.; Hens, Z. Highly Dynamic Ligand Binding and Light Absorption Coefficient of Cesium Lead Bromide Perovskite Nanocrystals. *ACS Nano* **2016**, *10*, 2071–2081.

(31) Zhang, F.; Huang, S.; Wang, P.; Chen, X.; Zhao, S.; Dong, Y.; Zhong, H. Colloidal Synthesis of Air-Stable $CH_3NH_3PbI_3$ Quantum Dots by Gaining Chemical Insight into the Solvent Effects. *Chem. Mater.* **2017**, *29*, 3793–3799.

(32) Li, X.; Li, H.; Bi, W.; Song, Y.; Ge, C.; Wang, A.; Wang, Z.; Hao, M.; Kang, Y.; Yang, Y.; Dong, Q. Hydration Intermediate Phase Regulated In-Plane and Out-Plane Epitaxy Growth of Oriented Nano-Array Structures on Perovskite Single Crystals. *Small* **2022**, *18*, 2107915.

(33) Grancini, G.; D'Innocenzo, V.; Dohner, E. R.; Martino, N.; Srimath Kandada, A. R.; Mosconi, E.; De Angelis, F.; Karunadasa, H. I.; Hoke, E. T.; Petrozza, A. $CH_3NH_3PbI_3$

Perovskite Single Crystals: Surface Photophysics and Their Interaction with the Environment. *Chem. Sci.* **2015**, *6*, 7305–7310.

(34) Nirmal, M.; Dabbousi, B. O.; Bawendi, M. G.; Macklin, J. J.; Trautman, J. K.; Harris, T. D.; Brus, L. E. Fluorescence Intermittency in Single Cadmium Selenide Nanocrystals. *Nature* **1996**, *383*, 802–804.

(35) Wen, X.; Ho-Baillie, A.; Huang, S.; Sheng, R.; Chen, S.; Ko, H.; Green, M. A. Mobile Charge-Induced Fluorescence Intermittency in Methylammonium Lead Bromide Perovskite. *Nano Lett.* **2015**, *15*, 4644–4649.

(36) Tian, Y.; Merdasa, A.; Peter, M.; Abdellah, M.; Zheng, K.; Ponseca, C. S.; Pullerits, T.; Yartsev, A.; Sundström, V.; Scheblykin, I. G. Giant Photoluminescence Blinking of Perovskite Nanocrystals Reveals Single-Trap Control of Luminescence. *Nano Lett.* **2015**, *15*, 1603–1608.

(37) Gerhard, M.; Louis, B.; Camacho, R.; Merdasa, A.; Li, J.; Kiligaridis, A.; Dobrovolsky, A.; Hofkens, J.; Scheblykin, I. G. Microscopic Insight into Non-Radiative Decay in Perovskite Semiconductors from Temperature-Dependent Luminescence Blinking. *Nat. Commun.* **2019**, *10*, 1698.

(38) Chouhan, L.; Ito, S.; Thomas, E. M.; Takano, Y.; Ghimire, S.; Miyasaka, H.; Biju, V. Real-Time Blinking Suppression of Perovskite Quantum Dots by Halide Vacancy Filling. *ACS Nano* **2021**, *15*, 2831–2838.

(39) Li, B.; Huang, H.; Zhang, G.; Yang, C.; Guo, W.; Chen, R.; Qin, C.; Gao, Y.; Biju, V. P.; Rogach, A. L.; Xiao, L.; Jia, S. Excitons and Biexciton Dynamics in Single $CsPbBr_3$ Perovskite Quantum Dots. *J. Phys. Chem. Lett.* **2018**, *9*, 6934–6940.

(40) Yuan, G.; Ritchie, C.; Ritter, M.; Murphy, S.; Gómez, D. E.; Mulvaney, P. The Degradation and Blinking of Single $CsPbI_3$ Perovskite Quantum Dots. *J. Phys. Chem. C* **2018**, *122*, 13407–13415.

(41) Wang, X.; Qu, L.; Zhang, J.; Peng, X.; Xiao, M. Surface-Related Emission in Highly Luminescent CdSe Quantum Dots. *Nano Lett.* **2003**, *3*, 1103–1106.

(42) Hu, L.; Feng, M.; Wang, X.; Liu, S.; Wu, J.; Yan, B.; Lu, W.; Wang, F.; Hu, J.-S.; Xue, D.-J. Solution-Processed Ge(II)-Based Chalcogenide Thin Films with Tunable Bandgaps for Photovoltaics. *Chem. Sci.* **2022**, *13*, 5944–5950.

(43) Kimura, Y.; Karimata, I.; Kobori, Y.; Tachikawa, T. Mechanistic Insights into Photochemical Reactions on $CH_3NH_3PbBr_3$ Perovskite Nanoparticles from Single-Particle Photoluminescence Spectroscopy. *ChemNanoMat* **2019**, *5*, 340–345.

(44) Scheidt, R. A.; Kerns, E.; Kamat, P. V. Interfacial Charge Transfer between Excited $CsPbBr_3$ Nanocrystals and TiO_2 : Charge Injection versus Photodegradation. *J. Phys. Chem. Lett.* **2018**, *9*, 5962–5969.

(45) Xing, G.; Mathews, N.; Sun, S.; Lim, S. S.; Lam, Y. M.; Grätzel, M.; Mhaisalkar, S.; Sum, T. C. Long-Range Balanced Electron- and Hole-Transport Lengths in Organic-Inorganic $CH_3NH_3PbI_3$. *Science* **2013**, *342*, 344–347.

(46) Serpetzoglou, E.; Konidakis, I.; Kakavelakis, G.; Maksudov, T.; Kymakis, E.; Stratakis, E. Improved Carrier Transport in Perovskite Solar Cells Probed by Femtosecond Transient Absorption Spectroscopy. *ACS Appl. Mater. Interfaces* **2017**, *9*, 43910–43919.

(47) Zhu, Z.; Ma, J.; Wang, Z.; Mu, C.; Fan, Z.; Du, L.; Bai, Y.; Fan, L.; Yan, H.; Phillips, D. L.; Yang, S. Efficiency Enhancement of Perovskite Solar Cells through Fast Electron Extraction: The Role of Graphene Quantum Dots. *J. Am. Chem. Soc.* **2014**, *136*, 3760–3763.

(48) Stowell, C. A.; Korgel, B. A. Iridium Nanocrystal Synthesis and Surface Coating-Dependent Catalytic Activity. *Nano Lett.* **2005**, *5*, 1203–1207.

(49) Zheng, Z.; Tachikawa, T.; Majima, T. Single-Particle Study of Pt-Modified Au Nanorods for Plasmon-Enhanced Hydrogen Generation in Visible to Near-Infrared Region. *J. Am. Chem. Soc.* **2014**, *136*, 6870–6873.

(50) DuBose, J. T.; Kamat, P. V. Efficacy of Perovskite Photocatalysis: Challenges to Overcome. *ACS Energy Lett.* **2022**, *7*, 1994–2011.

(51) Dung, D.; Ramsden, J.; Grätzel, M. Dynamics of Interfacial Electron-Transfer Processes in Colloidal Semiconductor Systems. *J. Am. Chem. Soc.* **1982**, *104*, 2977–2985.

(52) Aristidou, N.; Eames, C.; Sanchez-Molina, I.; Bu, X.; Kosco, J.; Islam, M. S.; Haque, S. A. Fast Oxygen Diffusion and Iodide Defects Mediate Oxygen-Induced Degradation of Perovskite Solar Cells. *Nat. Commun.* **2017**, *8*, 15218.

(53) Peterson, J. J.; Nesbitt, D. J. Modified Power Law Behavior in Quantum Dot Blinking: A Novel Role for Biexcitons and Auger Ionization. *Nano Lett.* **2009**, *9*, 338–345.

(54) Yuan, G.; Gómez, D. E.; Kirkwood, N.; Boldt, K.; Mulvaney, P. Two Mechanisms Determine Quantum Dot Blinking. *ACS Nano* **2018**, *12*, 3397–3405.

(55) Xu, W.; Kong, J. S.; Yeh, Y.-T. E.; Chen, P. Single-Molecule Nanocatalysis Reveals Heterogeneous Reaction Pathways and Catalytic Dynamics. *Nat. Mater.* **2008**, *7*, 992–996.

(56) Tachikawa, T.; Yamashita, S.; Majima, T. Evidence for Crystal-Face-Dependent TiO_2 Photocatalysis from Single-Molecule Imaging and Kinetic Analysis. *J. Am. Chem. Soc.* **2011**, *133*, 7197–7204.